DOI: 10.1002/ejic.201000972

Influence of a Redox-Active Phosphane Ligand on the Oxidations of a Diiron Core Related to the Active Site of Fe-Only Hydrogenase

Yu-Chiao Liu,[a] Chia-Hsin Lee,[a] Gene-Hsiang Lee,[b] and Ming-Hsi Chiang*[a]

Keywords: Fe-only hydrogenases / Metalloenzymes / Electrochemistry / Iron / Phosphane ligands

Modulation of the Fe redox levels within the diiron dithiolato carbonyls with the coordination of a redox-active phosphane is reported. Treatment of $[Fe_2\{\mu\text{-}S(CH_2)_2NR(CH_2)_2S\}(CO)_6]_2$ and $[Fe_2(\mu\text{-pdt})(CO)_6]$ with mppf affords the phosphane substituted species, $[Fe_2\{\mu\text{-}S(CH_2)_2NR(CH_2)_2S\}(CO)_5(mppf)]_2$ (**1** and **2**) and $[Fe_2(\mu\text{-pdt})(CO)_5(mppf)]$ (**3**), respectively. These mppf-substituted complexes have been structurally and spectroscopically characterized. Results of the electrochemical study on **1** and **2** indicate that oxidation of the mppf-substituted complexes occurs at a potential 100 mV less than the related species ligated by the redox-inactive phosphane with approximately the same σ-donating ability. Stability of the oxidized species is improved on the electrochemical time scale. For the complex **3**, three reversible oxidation events are observed. The mppf unit is oxidized at 0.16 V, which exerts an influence on the oxidation potential of the diiron core. In contrast to the PPh_3 analogue, oxidation of both Fe centers is accessible at 0.47 and 0.77 V for **3**. A large $\Delta E_{1/2}$ value suggests a substantial electron delocalization within the Fe_2 core.

Introduction

An important function of Fe-only hydrogenase is energy cycling in biological systems.[1,2] It can either store reducing power in the form of molecular hydrogen or metabolize hydrogen molecules to generate reducing equivalents.[3] When protons are transported through the proton channel to the catalytic metal site, electrons are transferred to the Fe^d for reduction.[4,5] In the reverse pathway, heterogeneous cleavage of hydrogen molecules assisted by the aza nitrogen cofactor facilitates generation of protons and hydrides. The latter initially coordinates to the Lewis acidic Fe center and then migrates to the neighboring Lewis basic sites, i.e. the N- and/or S-containing residues, in concert with reduction of the metal center.[6,7] In both forward and reverse reactions, the determining role that mediates electron flux shuttling between the active site and the rest of the protein is the ferredoxin cluster that is covalently bonded to the $[Fe_2S_2]$ subset through a cysteinyl thiolate on the peptide chain (Scheme 1).[8,9]

Electronic communication between two linked units, the [4Fe4S] cluster and the $[Fe_2S_2]$ subset, was first attested by Pickett et al.[10] It was shown that the reduction potential of the [4Fe4S] cluster in $[Fe_4S_4(L)(Fe_2\{CH_3C(CH_2S)_3\}\{CO\}_5)][NBu_4]_2$ {L = 1,3,5-tris(4,6-dimethyl-3-mercaptophenylthio)-2,4,6-tris(*p*-tolylthio)benzene} is positively

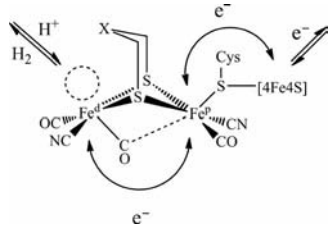

Scheme 1. The proton–electron transfer pathway within the active site of Fe-only hydrogenase.

shifted by 120 mV to –0.86 V compared to the unattached analogue. Intramolecular electron transfer from the reduced cubane to the Fe_2 subset, suggesting interplay of redox states between two units, is evidenced from a simulated mechanism and generation of the detached [4Fe4S] cluster in the oxidized form.

It is of interest to examine a $\{Fe_2S_2\}$–mppf system [mppf = $(C_5H_5)Fe(C_5H_4PPh_2)$]. We designed this system for the following reasons: an irreversible oxidation proceeds at about 0.75 V (vs. Fc/Fc^+) for both $[Fe_2\{\mu\text{-}S(CH_2)_2NR(CH_2)_2S\}(CO)_6]_2$ and $[Fe_2(\mu\text{-pdt})(CO)_6]$ (pdt = 1,3-propanedithiolate).[11–16] The potential decreases by about 300 mV when the CO is replaced by one phosphane while irreversibility of the redox process persists. In addition, mppf is a redox-active phosphane ligand and its single-electron oxidation at 0.14 V is reversible.[17] Decrease of the potential difference between these two closely separated oxidation energy levels upon coordination of mppf to the Fe_2 core could facilitate electron transfer in between and provide an avenue to direct observation of the influence of an

[a] Institute of Chemistry, Academia Sinica, Nankang, Taipei 115, Taiwan
E-mail: mhchiang@chem.sinica.edu.tw
[b] Instrumentation Center, National Taiwan University, Taipei 106, Taiwan
Supporting information for this article is available on the WWW under http://dx.doi.org/10.1002/ejic.201000972.

attached redox-active fragment on the Fe oxidation potential.

Previously, we have reported preparation of $[Fe_2\{\mu\text{-}S(CH_2)_2NR(CH_2)_2S\}(CO)_6]_2$ and $[Fe_2\{\mu\text{-}S(CH_2)_2NR(CH_2)_2S\}(CO)_5(PPh_3)]_2$.[11] The electrochemical properties of these complexes have been studied. The syntheses and electrochemistry of the pdt analogues are well documented.[12–16] $[Fe_2(\mu\text{-}x\text{dt})(CO)_5(\text{mppf})]$ (x = *N*-*p*-$C_6H_4CH_3$, S) have been synthesized and the adt [adt = $(p\text{-}C_6H_4CH_3)N(CH_2S^-)_2$] derivative has been structurally characterized.[18,19] However, none of these compounds have been explored electrochemically. Herein, we report the synthesis and characterization of $[Fe_2\{\mu\text{-}S(CH_2)_2NR(CH_2)_2S\}(CO)_5(\text{mppf})]_2$ and $[Fe_2(\mu\text{-pdt})(CO)_5(\text{mppf})]$. Similar ν(CO) band energies are observed for the PPh_3- and mppf-substituted species. By choosing phosphane ligands with approximately the same σ-donating ability, the role of redox-active ligands on the HOMO of the Fe_2 core can be disentangled. It is concluded that distinct electrochemical features in $[Fe_2\{\mu\text{-}S(CH_2)_2NR(CH_2)_2S\}(CO)_5(\text{mppf})]_2$ and $[Fe_2(\mu\text{-pdt})(CO)_5(\text{mppf})]$ can be ascribed to the involvement of redox orbitals of mppf with those of the $\{Fe_2S_2\}$ unit.

Results and Discussion

Synthesis and Characterization of 1–3

When a toluene solution of $[Fe_2\{\mu\text{-}S(CH_2)_2NR(CH_2)_2S\}(CO)_6]_2$ (R = *i*Pr, *n*Pr) was treated with mppf in the presence of Me_3NO at ambient temperature, *cis*-$[Fe_2\{\mu\text{-}S(CH_2)_2NR(CH_2)_2S\}(CO)_5(\text{mppf})]_2$ (R = *i*Pr, *cis*-**1**; *n*Pr, *cis*-**2**) was isolated as a major product in solution, accompanied by some precipitation of the *trans* species as a minor product (< 10%). Identification of the complexes was made by the IR signatures: 2045 s, 1978 vs, 1956 sh, 1923 w and 2046 s, 1978 vs, 1957 sh, 1923 w cm^{-1} in CH_2Cl_2 solution for *cis*-**1** and *cis*-**2**, respectively. The *trans* isomer was obtained as the sole product when the reaction was performed with heating (Scheme 2). The relatively low solubility of the *trans* species in common organic solvents makes the isolation easy but limits characterization and electrochemical investigation in solution. A similar synthetic procedure was employed to generate $[Fe_2(\mu\text{-pdt})(CO)_5(\text{mppf})]$ (**3**). Its IR peak pattern is identical to that of **1** and **2**, suggesting that they all have the same $\{Fe_2S_2\}$ structural core. Energies of the IR peaks

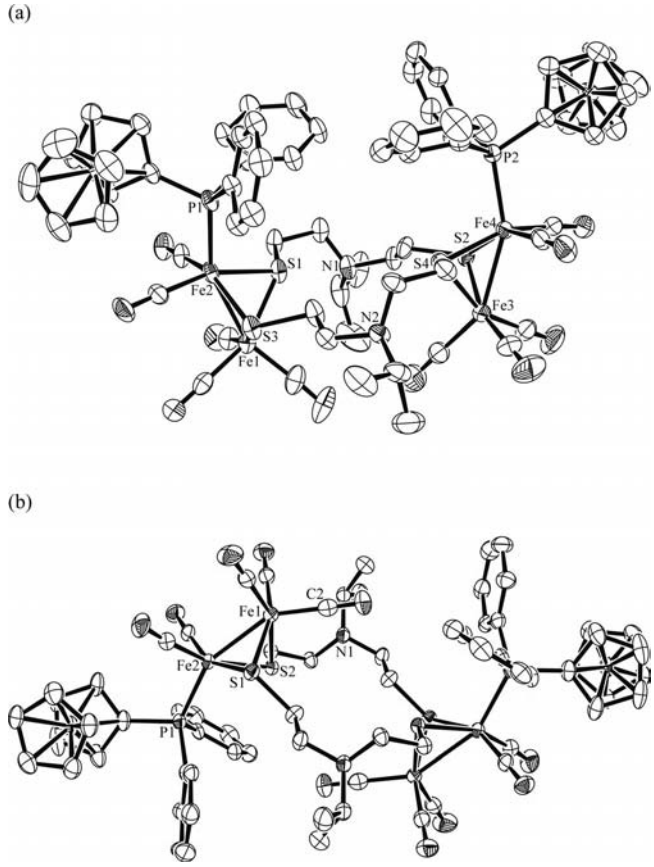

Figure 1. Molecular structures of (a) *cis*-**1** with thermal ellipsoids drawn at the 30% probability level and (b) *trans*-**1** with thermal ellipsoids drawn at the 50% probability level. Hydrogen atoms are omitted for clarity. Selected bond lengths [Å] and angles [°] for *cis*-**1**: Fe–Fe, 2.5005(8); Fe–S, 2.2689(11); Fe–P, 2.2226(12); Fe–$C_{CO,ap}$, 1.811(9); Fe–$C_{CO,ba}$, 1.775(4); S–Fe–S, 79.74(4); S–Fe–Fe, 56.56(3); Fe–S–Fe, 66.88(3); *trans*-**1**: Fe–Fe, 2.5093(9); Fe–S, 2.2710(13); Fe–P, 2.2343(14); Fe–$C_{CO,ap}$, 1.822(6); Fe–$C_{CO,ba}$, 1.777(5); S–Fe–S, 79.37(5); S–Fe–Fe, 56.46(4); Fe–S–Fe, 67.07(4).

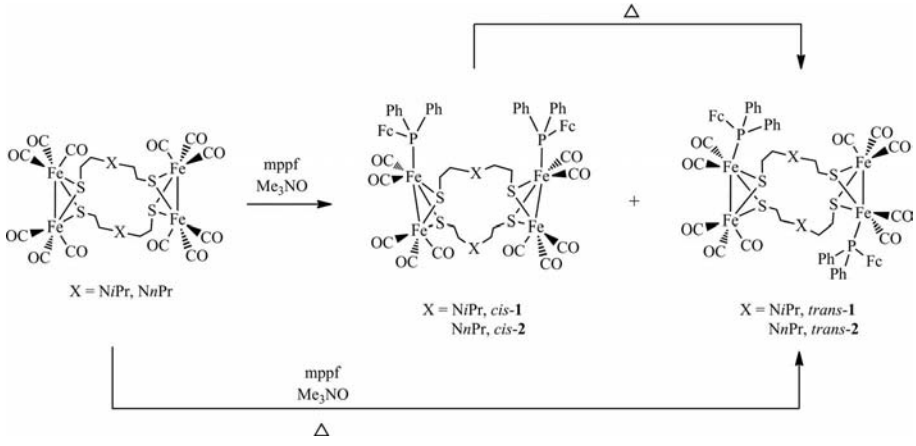

Scheme 2. Reaction scheme for the synthesis of **1** and **2**.

of the complexes **1**–**3** reveal no significant difference from those of their PPh_3 derivatives. This suggests that PPh_3 and mppf have approximately the same donor strength. The molecular structures of the complexes *cis*-**1** and *trans*-**1** are shown in Figure 1 and that of *cis*-**2** in Figure S1. Figure 2 displays the molecular structure of **3**. Selected metric parameters are listed in the figure captions. No significant variation for the mppf species is observed compared to their PPh_3 analogues.

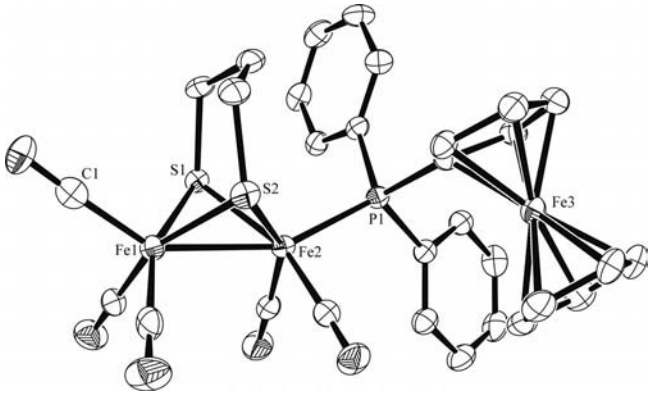

Figure 2. Molecular structure of **3**, with thermal ellipsoids drawn at the 50% probability level. Hydrogen atoms are omitted for clarity. Selected bond lengths [Å] and angles [°]: Fe–Fe, 2.5170(9); Fe–S, 2.2638(13); Fe–P, 2.2377(13); Fe–$C_{CO,ap}$, 1.805(6); Fe–$C_{CO,ba}$, 1.781(5); S–Fe–S, 84.66(5); S–Fe–Fe, 56.23(4); Fe–S–Fe, 67.55(4).

Two different behaviors in the $^{31}P\{^1H\}$ NMR spectra are observed for the adt and pdt species in CD_2Cl_2. For the complexes *cis*-**1**, and *cis*-**2**, a single resonance remains in the temperature range of 300–183 K. The signal broadens at T ≈ 230 K and becomes sharp again at lower temperature suggesting the presence of only one species. The ^{31}P NMR spectra of **3** reveal significant temperature dependence (Figure 3). The singlet of 55.9 ppm broadens upon cooling. The appearance of two new signals at δ = 51.6 and 63.1 ppm with unequal integrations suggests that three isomers are present, resulting from the apical/basal fluxional process along with the flipping process of the methylene bridgehead. From the ratio of 1 (δ = 63.1 ppm):21 (δ = 54.2 ppm):6 (δ = 51.6 ppm) it can be seen that the major species in the solution preserves its structure in the solid state.

Conversion of the kinetic species, *cis*, to the thermodynamic product, *trans*, was monitored by IR and ^{31}P NMR spectroscopy. Figure 4 displays the IR spectral changes with time for the toluene solution of *cis*-**1** at 80 °C. The IR bands of *cis*-**1** decreased in concert with the precipitation of *trans*-**1**. When the conversion process was complete, the solution color became pale orange and most of the *trans*-**1** product was present in solid form. A longer reaction time was required for the reaction proceeded at room temperature. No intermediate was observed during the conversion.

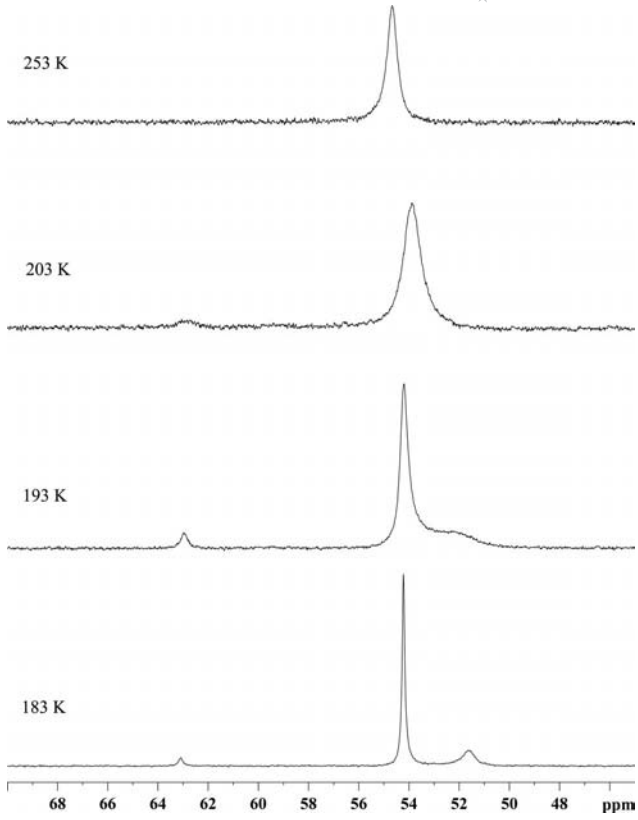

Figure 3. $^{31}P\{^1H\}$ NMR spectra of **3** in the CD_2Cl_2 solution at various temperatures.

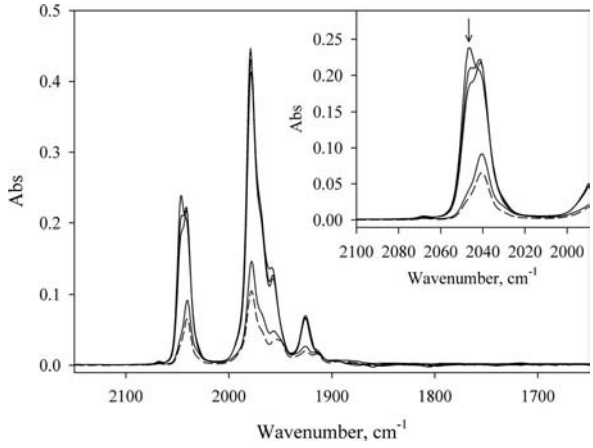

Figure 4. FTIR spectral changes for the conversion of *cis*-**1** to *trans*-**1** in the hot toluene solution. The spectrum inset highlights the IR region between 2100 and 1990 cm^{-1}. The short dashed lines indicate the signals of *trans*-**1**.

Electrochemistry

Cyclic voltammograms of *cis*-**1** and *cis*-**2** in the accessible electrochemical window of the CH_2Cl_2 solution at ambient temperature under N_2 exhibits one irreversible redox event at –2.19 and –2.18 V (all potentials are referenced to Fc/Fc^+) for *cis*-**1** and *cis*-**2**, respectively, which are assigned to the reduction of these complexes (Figure 5). These reduction potentials are comparable to that of –2.17 V for

Table 1. Electrochemical properties of **1**–**3** (1 mM, 0.1 M nBu$_4$NPF$_6$, υ = 100 mV/s) and related compounds.

Complex	Solvent	E_{pa}[a]	E_{pc}[a]
[Fe$_2${μ-S(CH$_2$)$_2$NnPr(CH$_2$)$_2$S}(CO)$_6$]$_2$	CH$_2$Cl$_2$[11]	+0.74	–1.90
[Fe$_2${μ-S(CH$_2$)$_2$NnPr(CH$_2$)$_2$S}(CO)$_5$(PPh$_3$)]$_2$	CH$_2$Cl$_2$[11]	+0.35	–2.17
cis-[Fe$_2${μ-S(CH$_2$)$_2$NiPr(CH$_2$)$_2$S}(CO)$_5$(mppf)]$_2$, *cis*-**1**	CH$_2$Cl$_2$	+0.46, +0.26(qr)	–2.19
cis-[Fe$_2${μ-S(CH$_2$)$_2$NnPr(CH$_2$)$_2$S}(CO)$_5$(mppf)]$_2$, *cis*-**2**	CH$_2$Cl$_2$	+0.44(qr), +0.27(qr)	–2.18
[Fe$_2$(μ-pdt)(CO)$_6$]	CH$_3$CN[13]	+0.74[b]	–1.74[b]
	CH$_3$CN[16]	+1.2[c]	–1.16(rv)[c]
	CH$_3$CN[14]	+0.84[d]	–1.57[d]
	CH$_3$CN[15]	+0.67[e]	–1.6[e]
	THF[16]	_[c]	–1.25(rv)[c]
	THF[12]	_[f]	–1.73[f]
	CH$_2$Cl$_2$	+0.84	–1.93
[Fe$_2$(μ-pdt)(CO)$_5$(PPh$_3$)]	CH$_3$CN[14]	+0.70, +0.34[d]	–1.76[d]
	CH$_2$Cl$_2$	+0.29(qr)	–2.12
	CH$_2$Cl$_2$	+0.32(rv)[g]	–2.04[g]
[Fe$_2$(μ-pdt)(CO)$_5$(mppf)], **3**	CH$_2$Cl$_2$	+0.53, +0.22(rv)	–2.04
	CH$_2$Cl$_2$	0.77(rv), 0.47(qr), 0.16(rv)[g]	–2.14[g]

[a] All redox pairs are irreversible and the potentials are referenced to Fc/Fc$^+$ unless noted otherwise. rv = reversible. qr = quasireversible. E_{pa} (or E_{pc}) = $E_{1/2}$ when the redox process is (quasi)reversible. [b] Under N$_2$ or CO, 0.1 M nBu$_4$NPF$_6$, υ = 200 mV/s. [c] nBu$_4$NPF$_6$, υ = 200 mV/s. The oxidation potential was not reported in THF. Referenced to Ag/AgCl. [d] 0.1 M nBu$_4$NPF$_6$, υ = 100 mV/s. Referenced to Ag/AgNO$_3$. [e] 0.3 M nBu$_4$NPF$_6$, υ = 100 mV/s. [f] Under N$_2$ or CO, 0.3 M nBu$_4$NClO$_4$, υ = 100 mV/s. The oxidation potential was not reported. [g] 0.1 M nBu$_4$NBArF$_{24}$, see text.

[Fe$_2${μ-S(CH$_2$)$_2$NnPr(CH$_2$)$_2$S}(CO)$_5$(PPh$_3$)]$_2$.[11] For the oxidation responses, two quasireversible processes are recorded. The first occurs at 0.26 and 0.27 V for *cis*-**1** and *cis*-**2**, respectively, and is assigned to the oxidation of mppf and one Fe center on the basis that mppf is oxidized at 0.1 V. The second Fe center is oxidized at 0.46 and 0.44 V for *cis*-**1** and *cis*-**2**, respectively. Table 1 tabulates the redox potentials of **1**–**3** and their analogues.

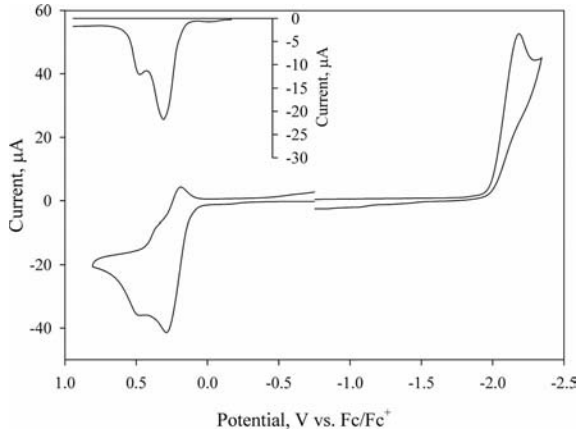

Figure 5. Cyclic voltammograms of *cis*-**2** (1 mM) in CH$_2$Cl$_2$ (υ = 100 mV/s, 0.1 M nBu$_4$NPF$_6$, vitreous carbon electrode) under N$_2$. Inset is shown the differential pulse voltammogram for the oxidation processes.

Complex **3** is reduced at –2.04 V in CH$_2$Cl$_2$ solution. When a positive potential is applied, oxidation of the mppf fragment at 0.22 V and a striping response at 0.53 V are observed (Figure 6a). Decomposition does not occur as reversibility of the mppf redox pair is sustained during adsorption and desorption of the oxidized species. Avoidance of the striping wave and disentanglement of the Fe oxidations are facilitated by the use of a weakly coordinating anion in CH$_2$Cl$_2$ solution. Three reversible oxidation and one irreversible reduction events are recorded when the voltammograms are measured in the presence of nBu$_4$NBArF$_{24}$ (BArF$_{24}$ = [B{C$_6$H$_3$(CF$_3$)$_2$}$_4$]$^-$) as a supporting electrolyte (Figure 6b). The reduction potential is slightly

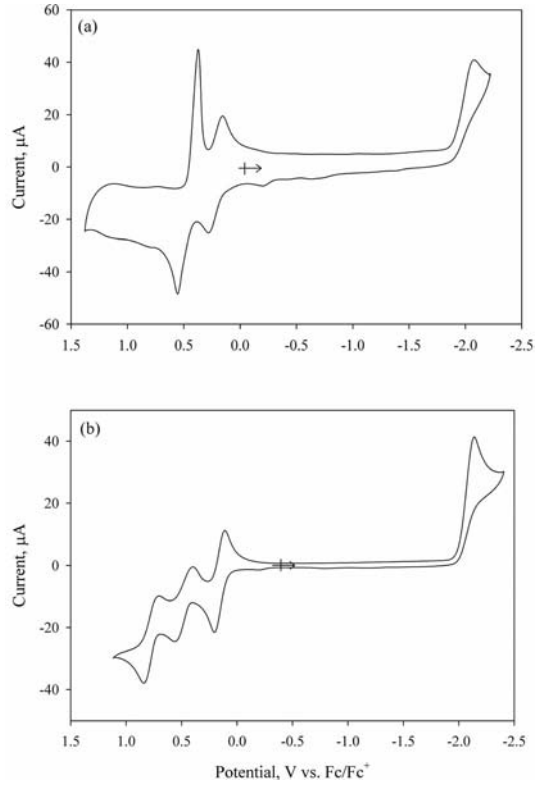

Figure 6. Cyclic voltammograms of **3** (1 mM) (a) in CH$_2$Cl$_2$ (υ = 225 mV/s, 0.1 M nBu$_4$NPF$_6$, vitreous carbon electrode) under N$_2$ and (b) in CH$_2$Cl$_2$ (υ = 100 mV/s, 0.1 M nBu$_4$NBArF$_{24}$, vitreous carbon electrode, 275 K) under N$_2$.

shifted to –2.14 V and its reversibility does not show any improvement. Two quasireversible oxidation events of the Fe centers at 0.47 and 0.77 V are resolved instead of absorption of the oxidized species. Likewise, the first oxidation at 0.16 V is a one-electron event ascribed to the Fe^{II}/Fe^{III} pair of mppf. The positive potential gain of 150 mV on average with respective to mppf for **1**–**3** suggests that the HOMO of mppf is substantially stabilized upon coordination to the $\{Fe_2S_2\}$ core. The $\Delta E_{1/2}$ shift recorded here compared to the observed result of 30 mV in $Re(CO)_4Cl$(mppf) reveals that the $\{Fe_2S_2\}$ core exerts a stronger electron-withdrawing effect.[17]

Electrocatalytic production of H_2 by **1**–**3** was monitored under N_2 with stepwise addition of acetic acid (HOAc). A new reduction wave was observed at the potential about 20–40 mV more positive when one equiv. of HOAc per $\{Fe_2S_2\}$ unit is added (Figure 7a and S2). The peak current of the reduction process increases linearly with sequential increments of acid added, indicating an electrocatalytic event (Figure 7b). The slopes of the I_c^{cat} vs. $[H^+]$/[complex] plots suggest that the efficiency of *cis*-**1** and *cis*-**2** for proton reduction catalysis is better than that of **3**. The rate constant

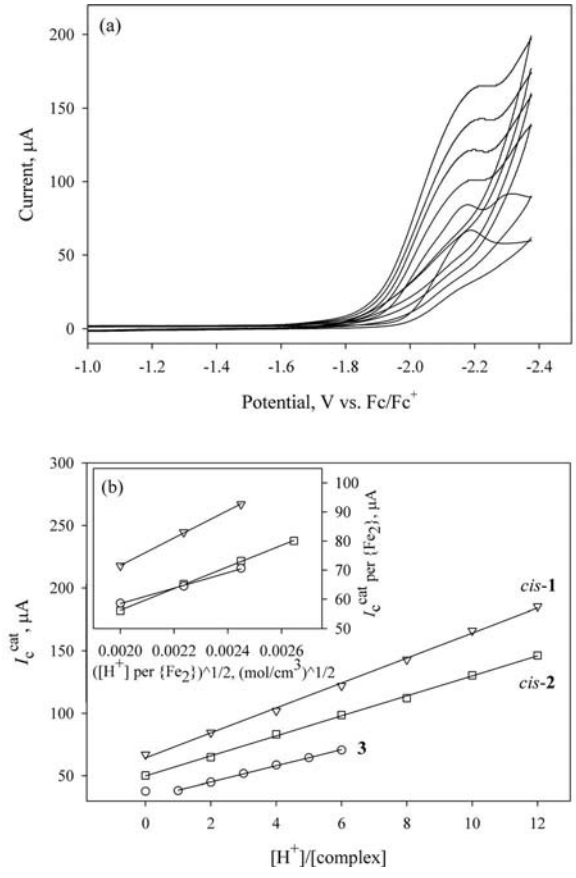

Figure 7. Cyclic voltammograms of (a) *cis*-**1** (1 mM) with increments of HOAc (0.0, 2.0, 4.0, 6.0, 8.0, and 10.0 equiv.) in CH_2Cl_2 (υ = 100 mV/s, 0.1 M nBu$_4$NPF$_6$, vitreous carbon electrode) under N_2. (b) Dependence of peak catalytic current (I_c^{cat}) vs. equiv. of HOAc added for **1**–**3** (at room temp. 1 mM in CH_2Cl_2). Inset is displayed the linear relationship between I_c^{cat} and the square root of the acid concentration per $\{Fe_2S_2\}$ unit.

is calculated from the plots of the I_c^{cat} vs. the square root of the acid concentration per $\{Fe_2S_2\}$ unit: $-I_c^{cat} = nFA[cat](D_{cat}{}^{1/2}k_{cat}{}^{1/2}[H^+]^{1/2}$ where I_c^{cat} is the catalytic current, n the number of electrons involved, F the Faraday constant, A the surface area of the working electrode, [cat] the bulk concentration of the catalyst, D_{cat} the diffusion coefficient of a catalyst, and k_{cat} the rate constant of the catalytic reaction.[20] The slope is proportional to $k_{cat}{}^{1/2}$ while the acid concentration is larger than the concentration of the catalyst. A good linear relationship is obtained with [HOAc]/[$\{Fe_2S_2\}$] > 3 for all complexes, shown in Figure 7b. The value of the $A[cat]D_{cat}{}^{1/2}$ product is calculated from the initial peak current prior to addition of acids. The rate constant k_{cat} for each $\{Fe_2S_2\}$ unit within *cis*-**1** and *cis*-**2** is estimated as 382 and 425 $M^{-1}s^{-1}$, respectively. Compared to the rate constant k_{cat} of 95 $M^{-1}s^{-1}$ for **3**, both *cis*-**1** and *cis*-**2** are superior catalysts to **3** with respect to reduction of HOAc to H_2.

Influence of the mppf Ligand

When **3** is chemically oxidized by 1 equiv. of [AcFc][BF_4] (AcFc = acetylferrocenium) or [AcFc][$BArF_{24}$] in CH_2Cl_2, the IR bands of the parent molecule are shifted to higher energies, as displayed in Figure S3. The average blueshift of 6 cm^{-1} (5 and 7 cm^{-1} for $[BF_4]^-$ and $[BArF_{24}]^-$, respectively) corresponds to the oxidation of the mppf fragment. The peak pattern for both the oxidized and parent species is identical. This indicates that single-electron oxidation causes no substantial change to the molecular structure of **3**.

The intriguing electrochemical feature of compounds **1**–**3** is that the two Fe centers within the $\{Fe_2S_2\}$ unit with ligation of mppf are oxidized at two separate potentials. These redox processes are quasireversible for **1** and **2** in the electrochemical timescale (υ = 100 mV/s), which is in marked contrast to that of their PPh_3 counterpart. [$Fe_2\{\mu$-$S(CH_2)_2N$*n*$Pr(CH_2)_2S\}(CO)_5(PPh_3)]_2$ exhibits one irreversible oxidation wave at 0.35 V under identical conditions. This value is closely matched to the average oxidation potential of 0.36 V for **1** and **2**.

Cyclic voltammograms of [$Fe_2(\mu$-pdt$)(CO)_5(PPh_3)$] were measured in CH_2Cl_2 for comparison. One irreversible reduction process of –2.12 V is observed, displayed in Figure S4. The oxidation is a quasireversible event occurring at 0.29 V. One redox process is recorded at more positive potential, which is due to the electrochemical response of the decomposed species that is suppressed at faster scan rates. Reversibility of the Fe^IFe^I/Fe^IFe^{II} redox pair is also improved under the same conditions. The Fe^IFe^I/Fe^IFe^{II} redox response is electrochemically reversible with substitution of the supporting electrolyte to nBu$_4$N$BArF_{24}$, shown in Figure S5. The current of the irreversible reduction is approximately twice that of the reversible oxidation, indicating the oxidation is a single-electron event in CH_2Cl_2.

Instead of one single-electron oxidation for the PPh_3 analogue, two one-electron oxidation events occur at 0.47 and 0.77 V for **3**. The presence of $[mppf]^+$ exerts an effect of 150 mV on the redox level of the Fe center within the

$\{Fe_2S_2\}$ unit with respect to the first Fe oxidation. In addition, ligation of mppf facilitates access to the $Fe^{II}Fe^{II}$ redox pair. Comproportionation constants (K_{comp}) of 2422 and 752 are calculated for *cis*-**1** and *cis*-**2**, respectively. These small values indicate that weak communication is present between two Fe centers. On the other hand, a large K_{comp} of 1.2×10^5 is obtained for **3**, suggesting substantial electron delocalization within the Fe_2 core. From these results it can be seen that access to further redox levels, namely oxidation, of the $\{Fe_2S_2\}$ unit benefits from the introduction of mppf. Experimental and theoretical investigations of the mixed valence and fully oxidized species are currently ongoing.

Conclusions

We have successfully used mppf as a simple model for the ferredoxin cluster in the H-cluster to examine the influence of a redox-active ligand on the redox levels of the Fe_2 subunit. Our results indicate that incorporation of mppf effectively alters the oxidation responses of the Fe centers without significant structural distortion. In addition, a substantial electron delocalization between the proximal and distal Fe sites is attested. These observations pave the way for the design of better artificial biocatalysts for hydrogen oxidation and production.

Experimental Section

General Methods: All reactions were carried out using standard Schlenk and vacuum line techniques under an atmosphere of purified nitrogen. All commercially available chemicals were of ACS grade and used without further purification. Solvents were of HPLC grade and purified as follows: diethyl ether and THF were distilled from sodium/benzophenone under N_2. Hexane was distilled from sodium under N_2. Dichloromethane was distilled from CaH_2 under N_2. Acetonitrile was distilled first over CaH_2 and then from P_2O_5 under N_2. Deuterated solvents obtained from Merck were distilled from 4 Å molecular sieves under N_2 prior to use. The preparation of $[Fe_2\{\mu\text{-}S(CH_2)_2NR(CH_2)_2S\}(CO)_6]_2$ (R = *i*Pr, *n*Pr) has been described previously.[11] [AcFc][BF_4],[21] Na[$BArF_{24}$],[22] Ag[$BArF_{24}$],[23] nBu_4NBArF_{24},[21] [AcFc][$BArF_{24}$],[21] [$Fe_2(\mu$-pdt)$(CO)_6$],[24] and mppf[25] were prepared according to the literature.

Infrared spectra were recorded with a Perkin–Elmer Spectrum One using a 0.05 mm CaF_2 cell. ^1H, $^{13}C\{^1H\}$ and $^{31}P\{^1H\}$ NMR spectra were recorded with a Bruker AV-500 or DRX-500 spectrometer operating at 500, 125.7, and 202.49 MHz. Spectra are referenced to tetramethylsilane (TMS) for ^1H and $^{13}C\{^1H\}$ and 85% H_3PO_4 for $^{31}P\{^1H\}$ NMR spectroscopy. Mass spectral analyses were performed with a Waters LCT Premier XE at the Mass Spectrometry Center in the Institute of Chemistry, Academia Sinica. Elemental analyses were performed with an Elementar vario EL III elemental analyzer.

Electrochemistry: Electrochemical measurements were recorded with a CH Instruments 630C electrochemical potentiostat using a gastight three-electrode cell under N_2. A glassy carbon electrode and a platinum wire were used as the working and auxiliary electrodes, respectively. The reference electrode was a nonaqueous Ag/Ag^+ electrode (0.01 M $AgNO_3$/0.1 M nBu_4NPF_6). All potentials are measured in 0.1 M nBu_4NPF_6 or nBu_4NBArF_{24} solution in CH_2Cl_2 and are reported against Fc/Fc^+.

Molecular Structure Determinations: The X-ray single crystal crystallographic data collections for **1**–**3** were carried out at 150 K with a Bruker SMART APEX CCD four-circle diffractometer with graphite-monochromated Mo-K_α radiation (λ = 0.71073 Å) outfitted with a low-temperature, nitrogen-stream aperture. The structures were solved by direct methods, in conjunction with standard difference Fourier techniques and refined by full-matrix least-squares procedures. A summary of the crystallographic data for the complexes **1**–**3** is shown in Table S1. An empirical absorption correction (multi-scan) was applied to the diffraction data for all structures. All non-hydrogen atoms were refined anisotropically and all hydrogen atoms were placed in geometrically calculated positions by the riding model. All software used for diffraction data processing and crystal structure solution and refinement are contained in the SHELXL-97 program suites.[26] One carbonyl group, C(6)O(6), and the cosolvent molecule, CH_2Cl_2, exhibit disorder in *cis*-**1**. In *trans*-**1**, the cosolvent CH_2Cl_2 exhibits disorder. The propyl group, C(17)–C(19), of the tertiary amine site is disordered in *cis*-**2**. There are two molecules in the unit cell of **3**, and two carbon atoms, C(37) and C(38), of the pdt bridge in one of the molecules are disordered.

Synthesis of *cis*-1: $[Fe_2\{\mu\text{-}S(CH_2)_2N\textit{i}Pr(CH_2)_2S\}(CO)_6]_2$ (400 mg, 0.44 mmol), mppf (375 mg, 1.01 mmol) and anhydrous Me_3NO (99 mg, 1.32 mmol) were placed in a 50 mL Schlenk flask in a dry box. Toluene (30 mL) was added to give an orange-red solution. The solution was stirred at ambient temperature for 1 h before the solvent was removed under reduced pressure. The solid was redissolved in CH_2Cl_2/acetone (v/v 10:1) and the solution was filtered through a silica gel plug. The filtrate was dried under vacuum to afford an orange-red solid which was washed with several portions of hexane. *cis*-$[Fe_2\{\mu\text{-}S(CH_2)_2N\textit{i}Pr(CH_2)_2S\}(CO)_5(mppf)]_2$ was obtained after purification by chromatography on silica gel with CH_2Cl_2 as the eluent. From the red band, an orange-red solid was obtained in 34% yield (237 mg). Crystals of *cis*-$[Fe_2\{\mu\text{-}S(CH_2)_2\text{-}N\textit{i}Pr(CH_2)_2S\}(CO)_5(mppf)]_2\cdot CH_2Cl_2$ suitable for X-ray crystallographic analysis were grown from a CH_2Cl_2/MeOH solution at –20 °C. IR (CH_2Cl_2): $\tilde{\nu}_{CO}$ = 2045 (s), 1978 (vs), 1956 (sh), 1923 (w) cm^{-1}. IR (KBr): $\tilde{\nu}_{CO}$ = 2044 (s), 1978 (vs), 1965 (s), 1954 (s), 1923 (m), 1895 (w, sh) cm^{-1}. ^1H NMR (500 MHz, CD_2Cl_2, 274 K): δ = 0.01 (br., 2 H, CH_2), 0.78 (d, $^3J_{HH}$ = 6.5 Hz, 6 H, 2 CH_3), 1.04 (d, $^3J_{HH}$ = 6.5 Hz, 6 H, 2 CH_3), 1.45 (m, 2 H, CH_2), 1.74 (t, $^3J_{HH}$ = 11.5 Hz, 2 H, CH_2), 1.97 (m, 4 H, 2 CH_2), 2.07 (m, 2 H, CH_2), 2.19 (m, 2 H, CH_2), 2.48 (hep, $^3J_{HH}$ = 6.5 Hz, 2 H, 2 NC*H*), 2.56 (m, 2 H, CH_2), 3.91 (s, 10 H, 2 Cp), 4.04 (s, 2 H, 2 PC_5H_4), 4.49 (s, 2 H, 2 PC_5H_4), 4.59 (s, 2 H, 2 PC_5H_4), 4.76 (s, 2 H, 2 PC_5H_4), 6.78–8.07 (20 H, 4 Ph) ppm. $^{13}C\{^1H\}$ NMR (125.7 MHz, CD_2Cl_2, 273 K): δ = 14.11 (2 *C*H_3), 21.05 (2 *C*H_3), 27.76 (2 *C*H_2), 37.91 (2 *C*H_2), 49.82 (*C*H_2 + 2 N*C*H), 49.89 (*C*H_2), 51.12 (2 *C*H_2), 70.17 (2 *C*$_5H_5$), 71.40, 71.47, 71.70, 72.92, 72.96, 76.70, 76.86, 79.04 (*ipso*), 79.44 (*ipso*) (2 P*C*$_5H_4$), 127.95, 128.02, 128.57, 128.62, 128.70, 131.03, 131.11, 135.08, 135.12, 135.22, 135.37, 141.48 (*ipso*), 141.81 (*ipso*) (4 Ph), 215.13, 215.19, 216.24, 216.29 (10 *C*O) ppm. $^{31}P\{^1H\}$ NMR (202.48 MHz, CD_2Cl_2, 273 K): δ = 54.65 (s) ppm. ESI-MS: *m*/*z* = 1486.76 {*cis*-**1** – 4CO + H^+}$^+$, 1599.75 {*cis*-**1** + H^+}$^+$. $C_{68}H_{68}Fe_6N_2O_{10}P_2S_4$ (1598.55): calcd. C 51.09, H 4.29, N 1.75; found C 51.01, H 4.61, N 1.70.

Synthesis of *cis*-2: A similar synthetic procedure was used as described above for *cis*-**1** with $[Fe_2\{\mu\text{-}S(CH_2)_2N\textit{n}Pr(CH_2)_2S\}(CO)_6]_2$ as the starting material. The yield was 77% yield (539 mg). Crystals

of *cis*-[Fe_2{μ-S(CH_2)$_2$N*n*Pr(CH_2)$_2$S}(CO)$_5$(mppf)]$_2$·CH_2Cl_2 suitable for X-ray crystallographic analysis were grown from a CH_2Cl_2/MeOH solution at –20 °C. IR (CH_2Cl_2): $\tilde{\nu}_{CO}$ = 2046 (s), 1978 (vs), 1957 (sh), 1923 (w) cm^{-1}. IR (KBr): $\tilde{\nu}_{CO}$ = 2042 (s), 1976 (vs), 1961 (s), 1952 (s), 1924 (m), 1897 (w, sh) cm^{-1}. ^{1}H NMR (500 MHz, CD_2Cl_2, 273 K): δ = 0.19 (br., 1 H, CH_2), 0.21 (br., 1 H, CH_2), 0.80 (t, $^3J_{HH}$ = 7.0 Hz, 6 H, 2 CH_3), 1.39 (m, 4 H, 2 NCH$_2$CH_2CH$_3$), 1.65 (m, 4 H, 2 CH_2), 1.82 (m, 4 H, 2 CH_2), 1.95 (m, 2 H, NCH_2CH$_2$CH$_3$), 2.09–2.21 (m, 4 H, CH_2 + NCH_2CH$_2$CH$_3$), 2.26 (m, 2 H, CH_2), 2.54 (m, 2 H, CH_2), 3.92 (s, 10 H, 2 Cp), 4.40 (s, 2 H, 2 PC$_5H_4$), 4.50 (s, 2 H, 2 PC$_5H_4$), 4.57 (s, 2 H, 2 PC$_5H_4$), 4.78 (s, 2 H, 2 PC$_5H_4$), 6.75–8.08 (20 H, 4 Ph) ppm. ^{13}C{^{1}H} NMR (125.7 MHz, CD_2Cl_2, 273 K): δ = 12.00 (2 *C*H$_3$), 19.63 (2 NCH$_2$*C*H$_2$CH$_3$), 25.66 (2 *C*H$_2$), 37.33 (2 *C*H$_2$), 54.44 (2 *C*H$_2$, overlapped with CD_2Cl_2), 56.20 (2 *C*H$_2$), 56.54 (2 N*C*H$_2$CH$_2$CH$_3$), 70.16 (2 *C*$_5$H$_5$), 71.41, 71.48, 71.76, 72.94, 72.97, 76.66, 76.82, 79.04 (*ipso*), 79.44 (*ipso*) (2 P*C*$_5$H$_4$), 127.93, 127.99, 128.61, 128.65, 128.73, 131.04, 131.11, 134.99, 135.10, 135.45, 141.50 (*ipso*), 141.83 (*ipso*) (4 Ph), 211.10 (br), 214.99, 215.06, 216.37, 216.42 (10 *C*O) ppm. ^{31}P{^{1}H} NMR (202.48 MHz, CD_2Cl_2, 273 K): δ = 54.43 (s) ppm. ESI-MS: *m*/*z* = 1485.89 {*cis*-**2** – 4CO + H^+}$^+$, 1570.88 {*cis*-**2** – CO + H^+}$^+$, 1598.78 {*cis*-**2** + H^+}$^+$. $C_{69}H_{70}Cl_2Fe_6N_2O_{10}P_2S_4$ (1683.49): calcd. C 49.23, H 4.19, N 1.66; found C 49.20, H 4.24, N 1.59.

Synthesis of *trans*-1: To a Schlenk flask containing [Fe_2{μ-S(CH_2)$_2$N*i*Pr(CH_2)$_2$S}(CO)$_6$]$_2$ (500 mg, 0.55 mmol) and mppf (446 mg, 1.20 mmol) was added toluene (15 mL). The solution was heated to 90 °C in an oil bath for 22 h. The solution was evaporated to dryness and several portions of hexane were used to wash the solid obtained. The solid was dried under vacuum and the yield was 86% (753 mg). Crystals of *trans*-[Fe_2{μ-S(CH_2)$_2$N*i*Pr(CH_2)$_2$S}(CO)$_5$(mppf)]$_2$·4CH_2Cl_2·H_2O suitable for X-ray crystallographic analysis were grown at –20 °C from a CH_2Cl_2/wet MeOH solution. IR (CH_2Cl_2): $\tilde{\nu}_{CO}$ = 2041 (s), 1978 (vs), 1966 (sh), 1957 (sh), 1921 (w) cm^{-1}. IR (KBr): $\tilde{\nu}_{CO}$ = 2040 (s), 1978 (s, sh), 1970 (vs), 1963 (s), 1951 (s), 1917 (m), 1899 (w, sh), 1890 (w, sh) cm^{-1}. ^{1}H NMR (500 MHz, CD_2Cl_2, 273 K): δ = 0.12 (m, 2 H, CH_2), 0.5 (d, $^3J_{HH}$ = 6.0 Hz, 6 H, 2 CH_3), 0.66 (d, $^3J_{HH}$ = 5.5 Hz, 6 H, 2 CH_3), 1.76 (m, 4 H, 2 CH_2), 1.95 (m, 6 H, 3 CH_2), 2.35 (m, 4 H, 2 NC*H* + CH_2), 2.48 (m, 2 H, CH_2), 3.93 (s, 10 H, 2 Cp), 4.04 (s, 2 H, 2 PC$_5H_4$), 4.47 (s, 2 H, 2 PC$_5H_4$), 4.60 (s, 2 H, 2 PC$_5H_4$), 4.74 (s, 2 H, 2 PC$_5H_4$), 7.09–8.06 (20 H, 4 Ph) ppm. ^{31}P{^{1}H} NMR (202.48 MHz, CD_2Cl_2, 273 K): δ = 54.78 (s) ppm. ESI-MS: *m*/*z* = 799.98 {*trans*-**1** + 2H^+}$^{2+}$, 1599.00 {*trans*-**1** + H^+}$^+$. $C_{68}H_{68}Fe_6N_2O_{10}P_2S_4$ (1598.55): calcd. C 51.09, H 4.29, N 1.75; found C 51.06, H 4.30, N 1.80.

Synthesis of *trans*-2: A similar synthetic procedure was used as described above for *trans*-**1** with [Fe_2{μ-S(CH_2)$_2$N*n*Pr(CH_2)$_2$S}(CO)$_6$]$_2$ as the starting material. The yield was 71% (621 mg). Attempts to grow crystals of *trans*-**2** were not made due to its very low solubility in organic solvents. IR (CH_2Cl_2): $\tilde{\nu}_{CO}$ = 2041 (s), 1978 (vs), 1955 (sh), 1919 (w) cm^{-1}. IR (KBr): $\tilde{\nu}_{CO}$ = 2034 (s), 1976 (s), 1957 (s), 1949 (s), 1926 (m), 1899 (w, sh) cm^{-1}. ^{31}P{^{1}H} NMR (202.48 MHz, CD_2Cl_2, 300 K): δ = 54.72 (s) ppm. ESI-MS: *m*/*z* = 1570.9 {*trans*-**2** – CO + H^+}$^+$, 1598.9 {*trans*-**2** + H^+}$^+$. $C_{68}H_{68}Fe_6N_2O_{10}P_2S_4$ (1598.55): calcd. C 51.09, H 4.29, N 1.75; found C 50.79, H 4.26, N 1.79.

Synthesis of 3: To a flask containing [Fe_2(μ-pdt)(CO)$_6$] (77 mg, 0.2 mmol) and Me_3NO·$2H_2O$ (22 mg, 0.2 mmol) was added CH_3CN (20 mL). An immediate color change to dark orange-brown was observed. The solution was stirred for half an hour before addition of mppf (74 mg, 0.2 mmol). The solution slowly turned to yellow-orange over 1.5 h. A red-orange-brown solid was obtained upon removal of the solvent under vacuum. The product was extracted from the solid by washing with THF/hexane. The solvent was removed from the extractant to afford an orange-red solid, which was purified by chromatography on silica gel with CH_2Cl_2/hexane (v/v 1:1) as the eluent to remove unreacted starting material and the second red-orange band was collected. Solvents were removed under reduced pressure to afford the red-orange solid of [Fe_2(μ-pdt)(CO)$_5$(mppf)] in 68% yield (99 mg). Crystals of [Fe_2(μ-pdt)(CO)$_5$(mppf)] suitable for X-ray crystallographic analysis were grown from a CH_2Cl_2/MeOH solution at –20 °C. IR (CH_2Cl_2): $\tilde{\nu}_{CO}$ = 2044 (s), 1981 (vs), 1960 (sh), 1930 (w) cm^{-1}. IR (KBr): $\tilde{\nu}_{CO}$ = 2050 (s), 2037 (m, sh), 1990 (m, sh), 1971 (vs), 1952 (s), 1930 (m), 1901 (w, sh) cm^{-1}. ^{1}H NMR (500 MHz, $CDCl_3$, 296 K): δ = 1.24 (m, 1 H, CH_2), 1.32 (m, 2 H, CH_2), 1.51 (m, 1 H, CH_2), 1.71 (m, 2 H, CH_2), 3.94 (s, 5 H, C$_5H_5$), 4.50 (m, 4 H, PC$_5H_4$), 7.40, 7.62 (m, 10 H, 2 Ph) ppm. ^{13}C{^{1}H} NMR (125.7 MHz, $CDCl_3$, 297 K): δ = 21.51 (2 *C*H$_2$), 29.94 (1 *C*H$_2$), 69.74 (*C*$_5$H$_5$), 71.22 (d, J_{PC} = 6.9 Hz, 2 C, P*C*$_5$H$_4$), 74.26 (d, J_{PC} = 11.6 Hz, 2 C, P*C*$_5$H$_4$), 78.66 (d, J_{PC} = 44.0 Hz, 1 C, *ipso*-P*C*$_5$H$_4$), 127.85 (d, J_{PC} = 9.6 Hz, 4 C, P*C*$_6$H$_5$), 129.72 (2 C, P*C*$_6$H$_5$), 132.95 (d, J_{PC} = 11.0 Hz, 4 C, P*C*$_6$H$_5$), 138.81 (d, J_{PC} = 42.7 Hz, 2 C, *ipso*-P*C*$_6$H$_5$), 209.53 (3 *C*O), 214.31 (d, J_{PC} = 10.9 Hz, 2 *C*O) ppm. ^{31}P{^{1}H} NMR (202.48 MHz, $CDCl_3$, 298 K): δ = 55.87 (s) ppm. FAB-MS: *m*/*z* = 728.0 {**3** + H^+}$^+$. $C_{30}H_{25}Fe_3O_5PS_2$ (728.16): calcd. C 49.48, H 3.46, S 8.81; found C 49.04, H 3.43, S 8.83.

Conversion of the *cis*-Isomers to the *trans*-Isomers: To a flask containing *cis*-**1** or *cis*-**2** (50 mg) was added toluene (10 mL). The solution was stirred at an elevated temperature and monitored constantly by FTIR spectroscopy. The length of conversion time depended on the reaction temperature. The reaction required 20 h for completion at 80 °C. When the reaction was finished, the pale yellow solution was removed. Several portions (3 mL × 3) of toluene were used to wash the remaining solid. The *trans*-isomers were obtained in yields greater than 80%. *cis*-**1**: IR (toluene): $\tilde{\nu}_{CO}$ = 2047 (s), 1979 (vs), 1969 (sh), 1958 (m), 1926 (w), 1915 (sh) cm^{-1}. *trans*-**1**: IR (toluene): $\tilde{\nu}_{CO}$ = 2040 (s), 1978 (vs), 1968 (sh), 1951 (m), 1925 (w), 1914 (sh) cm^{-1}. *cis*-**2**: IR (toluene): $\tilde{\nu}_{CO}$ = 2047 (s), 1980 (vs), 1970 (sh), 1959 (m), 1926 (w) cm^{-1}. *trans*-**2**: IR (toluene): $\tilde{\nu}_{CO}$ = 2041 (s), 1978 (vs), 1967 (sh), 1955 (m), 1926 (w) cm^{-1}.

Oxidation of 3 by [AcFc][BF_4] and [AcFc][$BArF_{24}$]: Chemical oxidation of **3** was conducted in CH_2Cl_2 under N_2 below –70 °C. When one equiv. of [AcFc][BF_4] or [AcFc][$BArF_{24}$] was added to the reaction solution, an instant color change to dark brown was observed. The in situ IR spectra were recorded with a Mettler Toledo ReactIR iC10 FTIR system equipped with a MCT detector and a 0.625 inch SiComp probe. The original IR peaks at 2044 (s), 1980 (vs), 1961 (sh), and 1931 (w) cm^{-1} were shifted to higher energies at 2050 (s), 1985 (vs), 1963 (sh), and 1931 (w) and 2053 (s), 1987 (vs), 1969 (sh), and 1931 (w) cm^{-1} for the [BF_4] and [$BArF_{24}$] salts, respectively. The IR band of 1662 cm^{-1} was assigned to the carbonyl group of acetylferrocene.

Supporting Information (see footnote on the first page of this article): Molecular structure of *cis*-**2**, cyclic voltammograms, IR spectra, and crystallographic data.

CCDC-792562 (for *cis*-**1**), -792563 (for *trans*-**1**), -792561 (for *cis*-**2**), and -792560 (for **3**) contain the supplementary crystallographic data for this paper. These data can be obtained free of charge from The Cambridge Crystallographic Data Centre via www.ccdc.cam.ac.uk/data_request/cif.

Acknowledgments

We are grateful to financial support from the National Science Council of Taiwan and Academia Sinica. We also thank Drs. Mei-Chun Tseng and Su-Ching Lin for help with MS analysis and 2D NMR spectroscopic experiments, respectively.

[1] P. M. Vignais, B. Billoud, *Chem. Rev.* **2007**, *107*, 4206–4272.
[2] K. A. Vincent, A. Parkin, F. A. Armstrong, *Chem. Rev.* **2007**, *107*, 4366–4413.
[3] J. C. Fontecilla-Camps, A. Volbeda, C. Cavazza, Y. Nicolet, *Chem. Rev.* **2007**, *107*, 4273–4303.
[4] J.-F. Capon, F. Gloaguen, F. Y. Pétillon, P. Schollhammer, J. Talarmin, *Coord. Chem. Rev.* **2009**, *253*, 1476–1494.
[5] F. Gloaguen, T. B. Rauchfuss, *Chem. Soc. Rev.* **2009**, *38*, 100–108.
[6] M.-H. Chiang, Y.-C. Liu, S.-T. Yang, G.-H. Lee, *Inorg. Chem.* **2009**, *48*, 7604–7612.
[7] P. E. M. Siegbahn, J. W. Tye, M. B. Hall, *Chem. Rev.* **2007**, *107*, 4414–4435.
[8] J. W. Peters, W. N. Lanzilotta, B. J. Lemon, L. C. Seefeldt, *Science* **1998**, *282*, 1853–1858.
[9] Y. Nicolet, C. Piras, P. Legrand, C. E. Hatchikian, J. C. Fontecilla-Camps, *Structure* **1999**, *7*, 13–23.
[10] C. Tard, X. Liu, S. K. Ibrahim, M. Bruschi, L. De Gioia, S. C. Davies, X. Yang, L.-S. Wang, G. Sawers, C. J. Pickett, *Nature* **2005**, *433*, 610–613.
[11] Y.-C. Liu, L.-K. Tu, T.-H. Yen, G.-H. Lee, S.-T. Yang, M.-H. Chiang, *Inorg. Chem.* **2010**, *49*, 6409–6420.
[12] S. J. Borg, T. Behrsing, S. P. Best, M. Razavet, X. Liu, C. J. Pickett, *J. Am. Chem. Soc.* **2004**, *126*, 16988–16999.
[13] D. Chong, I. P. Georgakaki, R. Mejia-Rodriguez, J. Sanabria-Chinchilla, M. P. Soriaga, M. Y. Darensbourg, *Dalton Trans.* **2003**, 4158–4163.
[14] P. Li, M. Wang, C. He, G. Li, X. Liu, C. Chen, B. Åkermark, L. Sun, *Eur. J. Inorg. Chem.* **2005**, 2506–2513.
[15] J. Ekström, M. Abrahamsson, C. Olson, J. Bergquist, B. Kaynak Filiz, L. Eriksson, L. Sun, H.-C. Becker, B. Åkermark, L. Hammarström, S. Ott, *Dalton Trans.* **2006**, 4599–4606.
[16] F. Gloaguen, J. D. Lawrence, M. Schmidt, S. R. Wilson, T. B. Rauchfuss, *J. Am. Chem. Soc.* **2001**, *123*, 12518–12527.
[17] T. M. Miller, K. J. Ahmed, M. S. Wrighton, *Inorg. Chem.* **1989**, *28*, 2347–2355.
[18] L.-C. Song, Q.-S. Li, Z.-Y. Yang, Y.-J. Hua, H.-Z. Bian, Q.-M. Hu, *Eur. J. Inorg. Chem.* **2010**, 1119–1128.
[19] Y. F. Tang, J. L. Zhu, *Acta Crystallogr., Sect. E* **2008**, *64*, m1423.
[20] A. J. Bard, L. R. Faulkner, *Electrochemical Methods: Fundamentals and Applications*, John Wiley & Sons, New York, **1980**.
[21] N. G. Connelly, W. E. Geiger, *Chem. Rev.* **1996**, *96*, 877–910.
[22] M. Brookhart, B. Grant, A. F. Volpe Jr., *Organometallics* **1992**, *11*, 3920–3922.
[23] Y. Hayashi, J. J. Rohde, E. J. Corey, *J. Am. Chem. Soc.* **1996**, *118*, 5502–5503.
[24] E. J. Lyon, I. P. Georgakaki, J. H. Reibenspies, M. Y. Darensbourg, *J. Am. Chem. Soc.* **2001**, *123*, 3268–3278.
[25] I. R. Butler, W. R. Cullen, *Organometallics* **1986**, *5*, 2537–2542.
[26] Bruker, ver. 6.10 ed., *Bruker Analytical X-Ray Systems*, Madison, WI, **2000**.

Received: September 13, 2010
Published Online: January 24, 2011

